



# Investigation of interfacial microstructure and mechanical characteristics of Ti/SS316 clads fabricated by explosive welding process

Bir Bahadur Sherpa<sup>1</sup> · Masatoshi Kuroda<sup>2</sup> · Tomohiro Ikeda<sup>3</sup> · Koji Kawamura<sup>3</sup> · Daisuke Inao<sup>4</sup> · Shigeru Tanaka<sup>1</sup> · Kazuyuki Hokamoto<sup>1</sup>

Received: 22 May 2023 / Accepted: 19 July 2023 / Published online: 26 July 2023  
© The Author(s), under exclusive licence to Springer-Verlag London Ltd., part of Springer Nature 2023

## Abstract

The study aimed to investigate the impact of varying stand-off distance (SOD) on the weld interface of pure titanium (Ti)/stainless steel (SS316) clads. Microstructural examination revealed a wavy interface morphology of welded clads. The morphological changes of the bonding interface under different SOD conditions showed that both the wavelength and amplitude increased with an increase in the SOD, with the wavelength demonstrating a more pronounced effect. In addition, a scratch test was also employed to characterize the weld interface. It is an important tool for evaluating the mechanical properties of a material. During scratch tests, an oval-shaped scratch morphology was observed on the Ti side, with the appearance of first divergent and then convergent behavior at the weld interface. In the tensile shear test, the Ti/SS316 clads exhibited higher tensile shear strength in the longitudinal direction compared to the transverse direction. The observed tensile shear strength values were in the range of 352.7–404.6 MPa for the longitudinal direction and 295.7–359.3 MPa for the transverse direction. The study found that the tensile shear strength increased in both the longitudinal and transverse directions as the SOD was increased from 5 to 10 mm. However, at an SOD of 15 mm, a decrease in tensile shear strength was observed in both directions. This decrease was attributed to the presence of non-uniform defects, such as cracks, voids, and high plastic deformation, at the interface zone. The fracture study revealed a combination of ductile and brittle fracture, with ductile fracture dominant at lower SOD and brittle fracture at higher SOD. The study found that the SOD had a substantial effect on the output of the weld results, and a SOD of 10 mm was determined to be the optimal welding parameter for Ti/SS316 clads based on microstructure and mechanical properties.

**Keywords** Stand-off distance · Weld interface · Ti · SS316 · Scratch test · Explosive welding

## 1 Introduction

Despite titanium's abundance as one of the most prevalent elements in the Earth's crust, it is classified as a rare metal. Over the past few decades, there has been a growing scientific and industrial interest in titanium attributed to its exceptional physical and chemical properties, such as superior corrosion resistance, high tensile strength, low density, and excellent biocompatibility [1]. These distinctive characteristics make titanium highly desired for diverse applications, particularly in the field of medical implants [2]. On the other hand, stainless steel, renowned for its passivation ability, high mechanical strength, remarkable thermal stability, and minimal susceptibility to environmental degradation, has found extensive utilization across various industrial sectors, including but not limited to laboratory equipment, food

✉ Kazuyuki Hokamoto  
hokamoto@mech.kumamoto-u.ac.jp

<sup>1</sup> Institute of Industrial Nanomaterials (IINa), Kumamoto University, Kumamoto 860-8555, Japan

<sup>2</sup> Faculty of Advanced Science and Technology, Kumamoto University, Kumamoto 860-8555, Japan

<sup>3</sup> Kumamoto Industrial Research Institute, Kumamoto 862-0901, Japan

<sup>4</sup> Faculty of Engineering, Kumamoto University, Kumamoto 860-8555, Japan

processing, and nuclear reactor [3]. In applications involving thick materials, the use of titanium as an individual material is too expensive. Thus, joining of titanium/steel plates provides a more cost-effective solution as it results in improved mechanical properties, enhanced corrosion resistance, and substantial cost reduction compared to using titanium alone. The bimetallic materials, consisting of two or more different materials, offer superior and manifold properties compared to single materials. However, conventional welding methods to manufacture titanium/steel clad plates are challenging due to dissimilarity in the metallurgical properties of titanium and steel, which leads to the formation of brittle intermetallic compounds at the welding interface [4]. In addition, the mechanical property incompatibilities between the two materials produce large residual stresses in the Ti/steel interface region, further degrading the bonding interface [5]. Currently, the primary methods for joining titanium and steel plates are vacuum brazing [6], laser welding [7], friction welding [8], oscillating laser welding [9], and pulsed laser welding [10]. However, unlike explosive welding, these methods are not efficiently applicable to large-area welding.

Explosive welding is a solid-state welding process that uses controlled explosives to create a high-pressure shock wave for cladding. It is well suited for welding similar and dissimilar materials due to its distinctive features, such as the capability to join large surface areas, the non-existence of a heat-affected zone (HAZ), and the fabrication of high-strength bonds. This welding technique is based on an explosive energy-driven mechanism, where the kinetic energy released during an explosion is applied to accelerate the flyer plate to strike with the base plate [11, 12]. The kinetic energy of the flyer plate is utilized to create high pressure in the weld zone upon impact, leading to a hydrodynamic flow of the metal surfaces in the impact region and resulting in solid-state bonding [13]. The energy released during an explosion is important for welding the two plates together, and this process enables the fabrication of composite materials that cannot be manufactured through conventional techniques [13, 14]. However, during explosive welding, a large amount of heat is produced at the weld interface, and there is insufficient time for heat dissipation. Moreover, the kinetic energy released during the collision causes partial melting and the formation of a local melted zone. To minimize the local melted zone in the bonded material, Hokamoto et al. [15] have initiated the use of an intermediate plate positioned between the flyer and base plate and witnessed that the energy lost during impact can be reduced by using an intermediate plate. Additionally, an improvement in both weld strength and the welding zone can be attained. Further, an investigation of other welding parameters was also executed by several researchers. Mousavi and Sartangi [16] conducted a study to analyze the impact of various loading ratios on the explosively welded Ti/304SS. Their findings

revealed that an increase in explosive loading ratio leads to an increase in the amplitude and wavelength of the wave. However, a substantial increase in the amount of melting zone was witnessed at the weld interface due to the simultaneous increase in collision pressure and plastic deformation with the increase in loading ratio. Prasanthi et al. [17] examined the influence of loading ratio on titanium grade 2 and mild steel explosive welding and witnessed the formation of a mixed zone in the front slope of the waves at high loading conditions, along with the formation of large vortices. Chu et al. [18] investigated the microstructural behavior of explosively welded pure titanium (T-1) and mild steel plate (Q345), both experimentally and numerically. A wavy structure interface with melted region in crest, resulted from a trapped jet, was observed. Zhou et al. [19] explosively welded Ti (TA2)/mild steel plates (Q235). The authors studied the microstructure of welded interface and observed straight to wavy and irregular interface morphology. Along with this non-uniform defects such as cracks, cavities, and brittle intermetallic were also observed. The mechanical properties of welded interface were significantly affected by the microstructure of weld interface. Previous research shows that successful joining of Ti/Steel and attaining good weld strength involves precise control of bonding conditions, as well as a thorough understanding of the microstructure and mechanical properties at the welding interface. Among various parameters effecting explosive welding, stand-off distance is quite crucial and can have substantial effect on the weld interface. However, no study have thoroughly investigated the effect of different SOD on the bond interface of titanium and steel bimetallics specifically stainless steel. Stainless steel (SS) is available in different grades such as SS304 and SS316 which are frequently used for various applications. However, SS316 can offer various industrial benefits over SS304. SS316 contains a higher nickel content than SS304 and 2–3% molybdenum, resulting in superior corrosion resistance compared to SS304, particularly in chloride environments that tend to cause pitting [20]. Therefore, this research aims to explosively weld titanium plate with SS316 and to examine the impact of different SOD on the microstructure and mechanical properties of the clad plates.

## 2 Materials and methods

Characterization of the interface of Ti/SS316 plates to study the effect of different SOD on microstructural and mechanical properties was performed using different mechanical tests, including the scratch test. The scratch test is a valuable tribological testing method for evaluating the performance characteristics of thin films, including their wear resistance and mechanical failure behavior. In this test, the indenter drags across the material's surface to create a scratch or

groove. The scratch test has also been employed in various fields, including coatings and thin films [21] to evaluate the adhesion strength and durability of the coating/film, microelectromechanical systems (MEMS) [22] to assess the mechanical reliability and tribological properties of micro-scale devices, and in biomedical devices [23] to evaluate the surface properties of implant materials and coatings. The scratch test has exhibited great potential to evaluate the surface properties of different materials. However, it has not been applied in the interface characterization and in examining the material behavior both near and across the weld interface in explosively welded samples. Our research findings have demonstrated the feasibility of using the scratch test to evaluate the interface bond of explosively welded samples and provide insights into the mechanical properties of the interface. Additionally, to comprehensively examine the quality of the explosively welded Ti/SS316 clads, the tensile shear strength was performed in two different directions, i.e., longitudinal and transverse directions. Moreover, the fracture morphology of the welded interface after the tensile shear test was thoroughly examined to elucidate the underlying mechanisms.

## 2.1 Experimental procedure

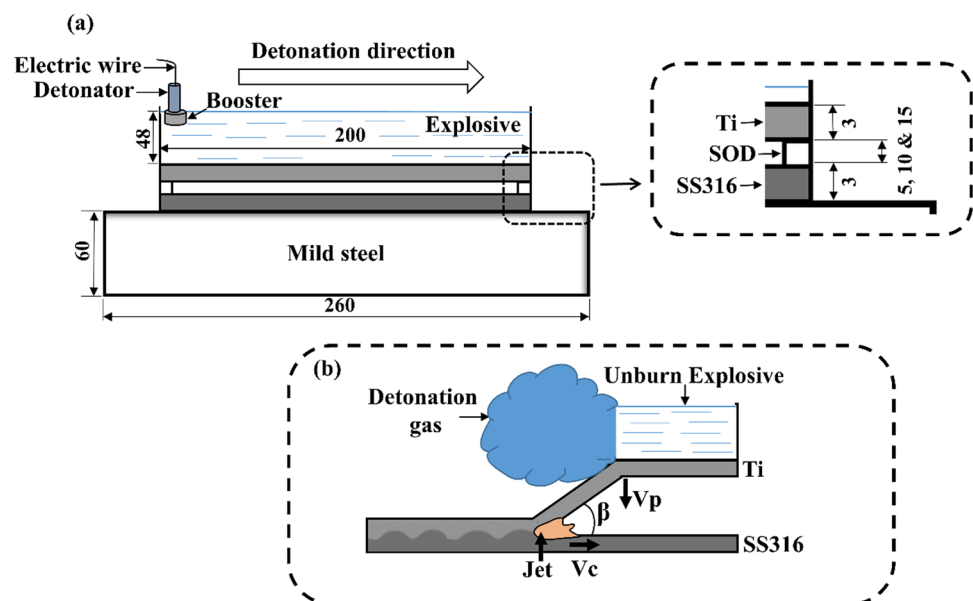
Ti/SS316 clads were fabricated using the parallel plate configuration method of the explosive welding process. The flyer plate used in the present study consisted of pure commercial titanium TP 270C, and SS316 stainless steel was used as a base plate. The dimensions of both the flyer and base plates were 200 mm × 100 mm × 3 mm. Both plates were gently cleaned and polished to achieve good surface bonding. The schematic representation of the experimental

setup for the explosive welding procedure is demonstrated in Fig. 1. The initial set-up before the experiment is shown in Fig. 1a, while Fig. 1b shows the explosive welding process at the intermediate stage. Here, the SS316 plate was placed on top of the anvil (mild steel), followed by the titanium plate. The two plates were separated by SOD, which was placed at a particular gap of 5 mm, 10 mm, and 15 mm for respective trials. The explosive used in the experiment was ANFO-A, which is a mixture of ammonium nitrate and fuel oil, having a density of 530 kg/m<sup>3</sup>. The initiation of the explosive was performed using a booster, composed of the high explosive SEP with a detonation velocity of 7 km/s and density of 1300 kg/m<sup>3</sup>. Furthermore, the booster was triggered by an electric detonator.

## 2.2 Microstructure analysis

For the microstructural analysis, specimens were prepared from the central region of the weld surface and were prepared in a plane parallel to the direction of explosive detonation. The specimens underwent grinding processes, where different sandpaper ranging from 400 to 1200 grit sizes were used. Subsequently, to enhance the quality of the results, the specimens were subjected to a polishing procedure applying abrasives ranging in size from 9.0 to 0.1 μm. To observe the grain structure near the weld interface of SS316, a solution comprising a 3:1 mixture of concentrated hydrochloric acid (HCl) and nitric acid (HNO<sub>3</sub>) was used for etching. The microstructural and morphological information of the interface was obtained using an optical microscope (Measurescope UM-2, Nikon) and scanning electron microscope (JCM-5700, JEOL Ltd), respectively. Furthermore, electron probe microanalysis (EPMA) was

**Fig. 1** Schematic view of explosive welding process: **a** initial set-up before the experiment; **b** at intermediate stage



used to evaluate the elemental composition of the interface for a comprehensive assessment of the element distribution in the interface zone.

### 2.3 Mechanical examination

The tensile shear strength of the bonded clads was measured using a similar method that was used by Xiang et al. [24]. The specimens were prepared using a wire-cutting machine with a wire diameter of 0.3 mm and were cut in both directions, i.e., longitudinal and transverse directions. The tensile shear test was carried out by a universal testing machine (UTM) (AG-250kNXplus, Shimadzu) with a loading speed of 0.1 mm/s. The experimental parameters are shown in Table 1. The microhardness examination was conducted on the weld interface using a Vickers hardness tester (HM-200, Mitsutoyo) to evaluate the hardness properties of the materials. The load applied for measuring the hardness of titanium and SS316 was 0.98 N. Scratch test was performed to evaluate the material property across the weld interface. The scratch test was conducted using the scratch tester (Anton Paar, RST<sup>3</sup> Revetest) with a constant applied load of 1 N,

**Table 1** Experimental parameters

Sample no.	Thick-ness of explosive (mm)	Stand-off distance (mm)	Thick-ness of flyer plate (mm)	Thick-ness of base plate (mm)	Welding results
1	48	5	3	3	Welded
2	48	10	3	3	Welded
3	48	15	3	3	Welded

a scratch length of 1000  $\mu\text{m}$ , an indenter radius of 200  $\mu\text{m}$ , and a speed of 2 mm/min. Overall, the microstructural analysis and the mechanical examination have provided valuable information on the material properties of the welded clads, which can aid in the evaluation of the quality and reliability of the welded structure.

## 3 Results and discussion

### 3.1 Microstructural examination

#### 3.1.1 Study of the weld interface

The typical micrographs of the bonding interface between pure titanium and SS316 are shown in Figs. 2 and 3. The figures show the presence of a wavy interface characteristic and periodic progression along the explosive welding direction. The formation of the wavy interface at the bonding zone is a significant hallmark of the explosive welding process and is consistent with Chu et al.'s study [25]. These findings further support the validity and consistency of the explosive welding process. The kinetic energy generated during the explosive welding process was sufficient to accelerate the flyer plate onto the base plate, resulting in substantial plastic deformation and the formation of a wavy interface. Examination of the micrographs showed the presence of a considerable local melted zone mainly at the front of the crest [18]. Etching the samples helps to reveal the grain structure behavior near the weld interface [26]. The grain structure of SS316 with an austenitic matrix is visible after etching. The grain structure exhibited significant elongation parallel

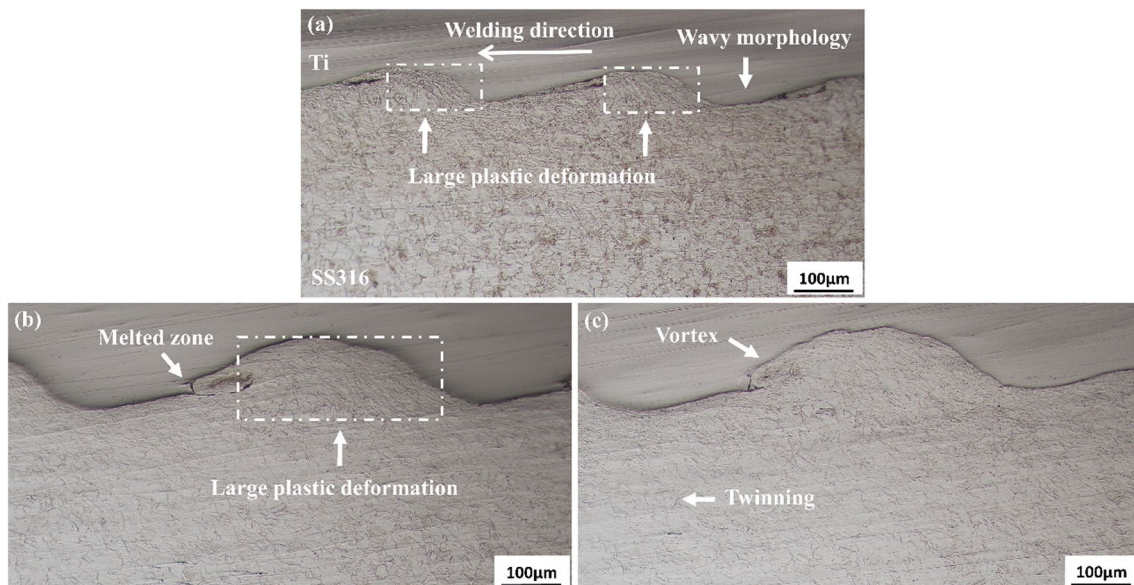
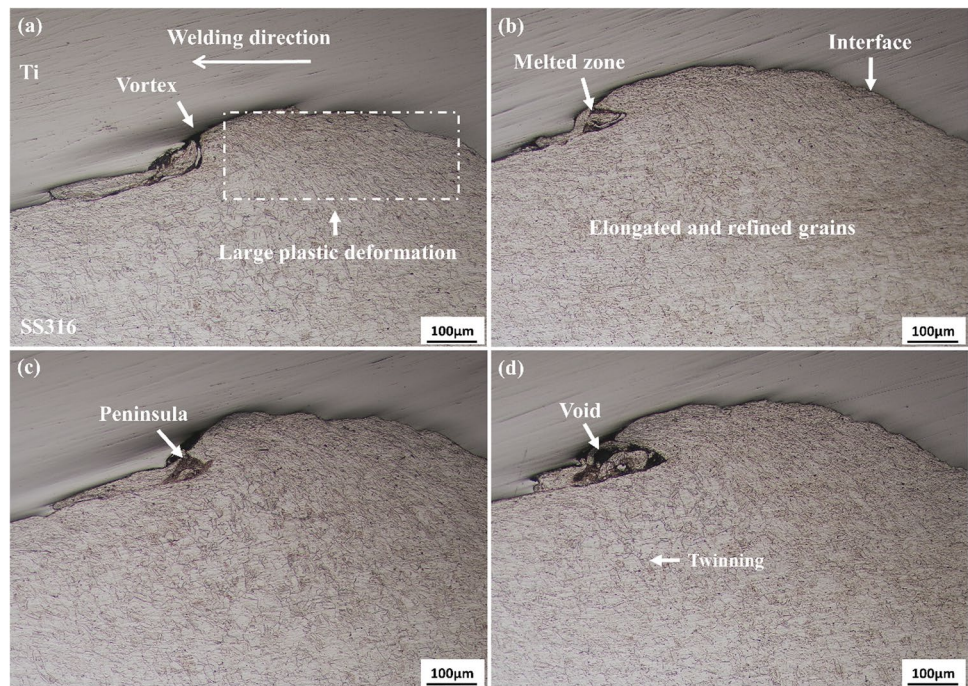


**Fig. 2** Optical microscopy images of Ti/SS316 weld interface: **a** sample 1; **b–c** sample 2

**Fig. 3** Optical microscopy images of Ti/SS316 weld interface: a–d sample 3



to the welding direction, indicating substantial deformation within the welding zone [27]. The vortex characteristics within the interface were clearly evident in the microstructure images. The vortex exhibited a periodic structure and was formed along the explosive welding direction at the interface wave front. Examination of the micrographs of the bonding interface at a low SOD-5 mm (Fig. 2a) revealed a clear, wavy interface at the weld zone. While at a SOD-10 mm (Fig. 2b, c) revealed a local melted zone at the weld interface with vortex formation. The energy released during the high-impact explosive welding process has resulted in friction, shearing of cladding materials, and high plastic deformation which are responsible for localized melting at the front vortex [28]. The formation of the vortex is due to the trapping of the jet. Bahrani et al. [29] have provided a clear explanation for this phenomenon, stating that the hump which is formed ahead of the collision point, deflects the jet upwards, and traps the re-entrant jet.

At SOD-15 mm (Fig. 3), a wavy morphology with vortices is observed. The increase in SOD results in the formation of melted zones ranging from 8 to 62 µm on the steel side due to partial melting. Figure 3c shows a typical microstructure having peninsula-type morphology on the SS316 side, which is commonly observed as a result of the combined action of the detonation force exerted by the explosive and the metal vortex flow [30]. Additionally, the formation of local melted zones can also be witnessed at the vortices of the bonding region. An increase in the SOD results in an increase in dynamic impact and kinetic energy. Similar results were also reported by Gloc et al. [31] in which

they have explosively welded titanium/low alloy steel and observed local melted zones with a thickness ranging from 5 to 70 µm. The cause of these local melted zones was due to the high kinetic energy present in the jet formed during the explosion. Yang et al. in their study explained the formation of a vortex structure with a molten pocket as a result of the combined actions of circular motion induced by shear instability and subsequent crest extrusion caused by hump growth [32].

### 3.1.2 Analysis of wavelength and amplitude at the weld interface

During the explosive welding process, the choice of parameters can lead to the formation of either a flat or wavy interface. However, the wavy interface is preferred over the flat one due to its superior bonding force, primarily attributed to the larger bonding area it offers [33]. The morphology of the wavy interface is significantly influenced by the propagation of plastic deformation ahead of the collision point [29]. Microstructural analysis, as demonstrated in Figs. 2 and 3, illustrates a direct relationship between the SOD and the waviness of the weld interface. Increasing the SOD results in an observable increment in the waviness. Specifically, specimens welded at SODs of 5 mm, 10 mm, and 15 mm exhibit bonding interfaces with wavelengths and amplitude of 339 µm and 63 µm, 731 µm and 155 µm, and 1200 µm and 179 µm, respectively. Notably, an increase in SOD leads to a simultaneous increase in both wavelength and amplitude. However, there is a more pronounced variation in

wavelength compared to amplitude with changes in SOD. This observation aligns with the previous research by Durgutlu et al. [34], where significantly higher wavelengths were reported for welds with higher SODs. Moreover, Fig. 4 validates the findings, showing that both wavelength and wave amplitude increase with higher SOD values. The mechanical locking of metals, resulting from increasing SOD, contributes to the enhanced bonding strength of the welded metals. Additionally, in the explosive welding process, an increase in explosive loading causes a rise in both wavelength and amplitude. Furthermore, an increase in impact velocity is directly associated with an increase in wavelength

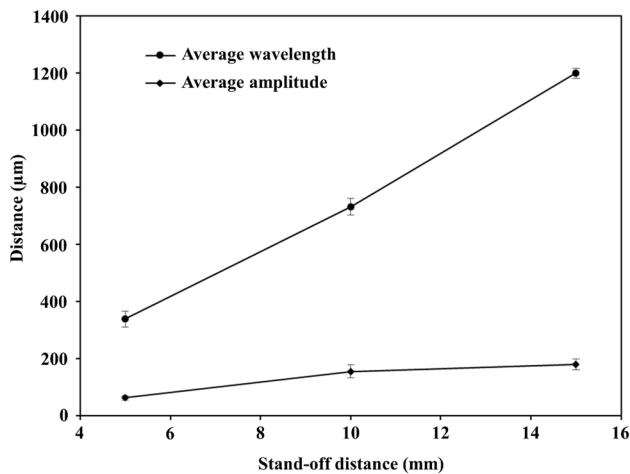


Fig. 4 Variation of wavelength and amplitude with stand-off distance

[16]. Wang et al. [35] in their study on explosively welded titanium and copper bimetals also observed a consistent relationship between SOD and the weld interface's waviness, where increasing SOD led to higher wavelength and amplitude.

### 3.1.3 EPMA of Ti/SS316

To analyze the bonding mechanism in specimens subjected to welding at varying SOD, EPMA was performed. The results obtained for the specimens welded at SOD-5 mm and SOD-10 mm are shown in Fig. 5, while those obtained for the specimen welded at SOD-15 mm are shown in Fig. 6. The EPMA was carried out to evaluate the distribution of Ti and Fe in the welding interface zone. The results obtained indicate the absence of any significant element diffusion into the adjacent matrix, except in the transition zones. At SOD-5 mm (Fig. 5a), a well-defined and uniform welding interface was observed. The two elements, Ti and Fe, were in their respective positions, and intermixing of elements was barely observed, indicating a uniform and defect-free bonding interface. The presence of a vortex formation at the bonding zone, as demonstrated in Fig. 5b, c, confirms the inter-diffusion of Ti and Fe elements at SOD-10 mm. EPMA conducted by Xiang et al. [24] showed that the vortex zone consisted of a complex composition, primarily of titanium, stainless steel, and Ti–Fe alloy phases. Manikandan et al. [36] observed the presence of dispersed FeTi and Fe<sub>2</sub>Ti intermetallic compounds within the vortex. Figure 6 depicts a more complex bonding microstructure at SOD-15

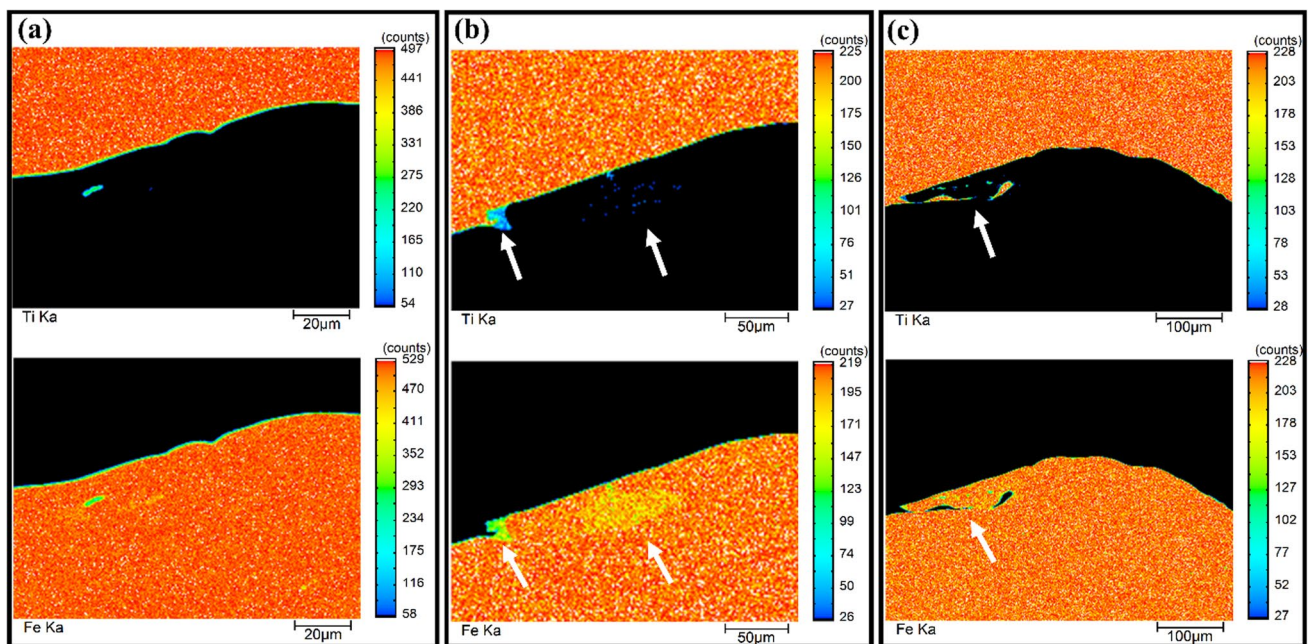
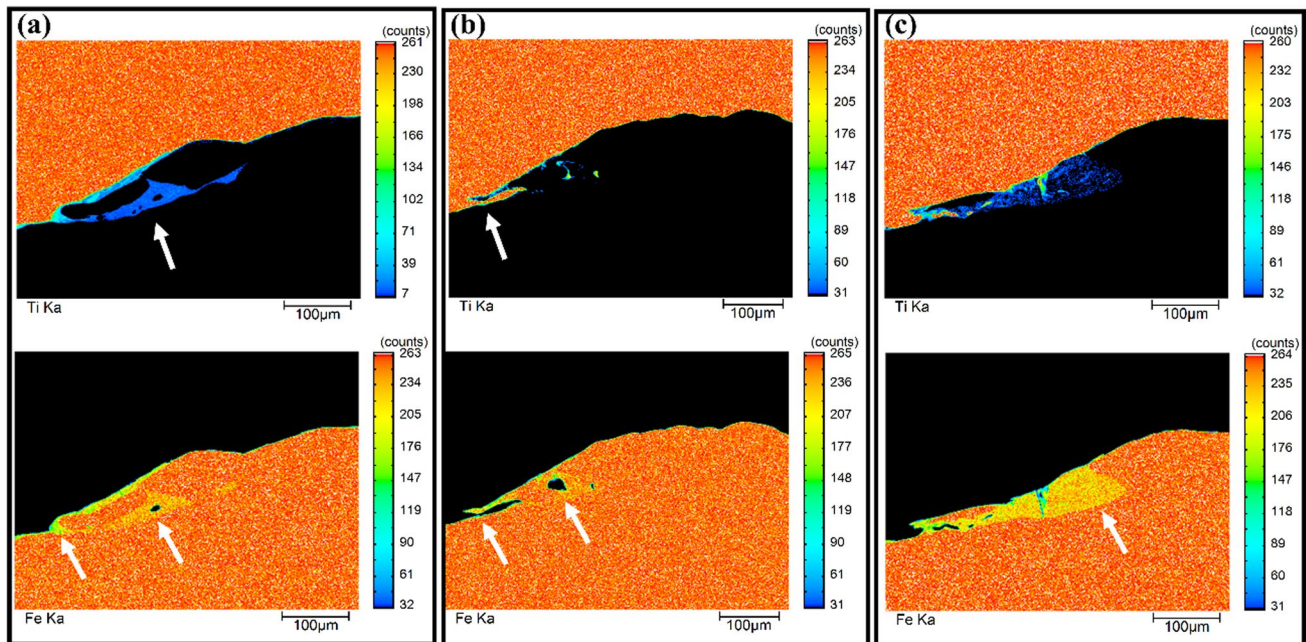


Fig. 5 EPMA results of Ti/SS316 weld interface: **a** sample 1; **b–c** sample 2



**Fig. 6** EPMA results of Ti/SS316 weld interface: **a–c** sample 3

mm, which is due to the presence of more intense vortex formation and defects. At higher SOD, the vortex exhibits localized melting at the wave front due to the heating of trapped jets. This is confirmed by the proper intermixing of Ti and Fe elements observed at the vortex, particularly the uniform intermixing observed at the tip of the wave front, as shown in Fig. 6a–c. Moreover, the vortex zone experiences a high cooling rate ranging between  $10^5$  and  $10^7$  K/s. As a result of this rapid quenching by the surrounding material, a melting pocket is formed within the vortex [36]. The thickness of the mixed zone for the specimen welded at SOD-15 mm was found to be large compared to that for the specimen welded at SOD-10 mm. This is due to the increase in pressure between the bonding plates and collision velocity as the SOD is increased [37]. Various defects such as porosity and microcracks were observed across the vortices. These defects were mainly due to the rapid solidification that occurs in the vortex region, characterized by an abrupt increase in temperature followed by high cooling rates [38]. As shown in Fig. 6c, it was also observed that the crack was initiated at the local melting zone, though it did not result in significant instability. The formation of fine grains during recrystallization has the ability of energy absorption which reduced the development of cracks [33]. Figure 6c clearly demonstrates the formation of island-like morphology in the vortex. The color of the islands is identical to that of the base metal, indicating that they are fragments of the base metal. The intense explosive detonation force and metal vortex flow resulted in the formation of this island-like morphology [30].

## 3.2 Mechanical examination

### 3.2.1 Hardness distribution study at the bonding interface

The Vickers microhardness test results are shown in Fig. 7. The microhardness examination was executed perpendicular to the weld interface to assess the hardness variation across the weld zone. In general, the weld interface experiences an increase in hardness value. However, in the present study, the microhardness values of the titanium side experienced a reduction near the weld interface (Fig. 7a). The decrease in microhardness values near the weld interface of the titanium side is due to the fact that Ti is comparatively softer than SS316. It is likely that most of the plastic deformation occurred only in the vortices of the flyer plate. This finding is consistent with the results reported by Chen et al. [39] where they have performed numerical simulations of TP 270/SUS821L1 and found that the percentage of jetting volume originating during welding was higher in the case of the Ti side. Paul et al. [40] have also demonstrated intense recovery, and recrystallization processes can result in reduced microhardness as the stored energy is the primary driving force for recrystallization, ultimately leading to material softening. On the other hand, SS316 revealed a distinct hardening behavior, with a sharp rise in hardness at the immediate vicinity of the weld interface, followed by a subsequent decline in hardness as one moves away from the weld interface. An increase in hardness value was observed due to work hardening and high levels of plastic deformation near the deformed area [41, 42]. Moreover, the current study

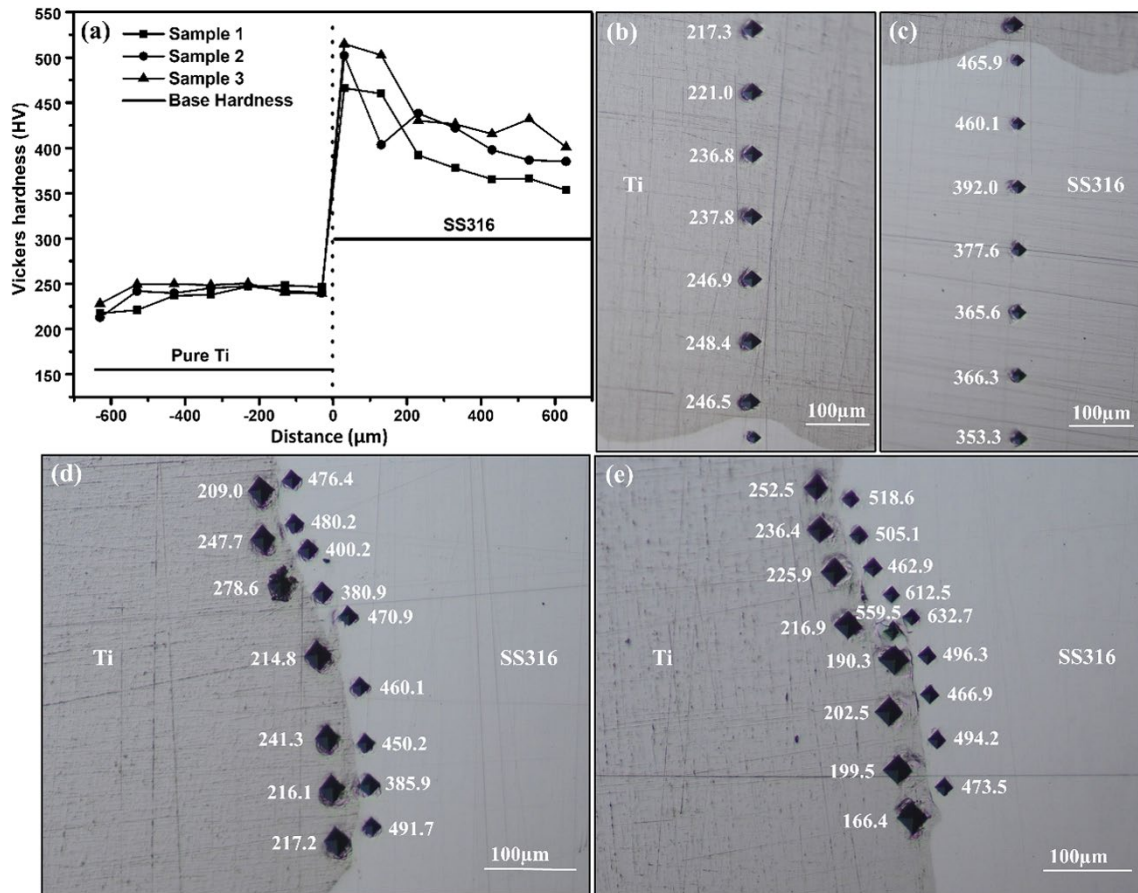


**Fig. 7** Microhardness results: **a** hardness profile across the weld interface; **b** sample 1, Ti side; **c** sample 1, SS316 side; **d** sample 2; **e** sample 3

witnessed that the variation in hardness value was larger on the SS316 side as compared to the Ti side, which was due to the greater work hardening effects during impact loading. This result is consistent with the earlier works reported by Zhao and Sheng [43] where they conducted a study on Ag/SS316L clad materials and reported an increase in hardness values at the weld interface. They further witnessed that the fluctuation and decreased amplitude of microhardness values on the 316L side were more pronounced than those on the Ag side. The observed phenomenon was due to grain refinement near the weld interface.

### 3.2.2 Scratch test for explosively welded Ti/SS316 clads

To explore the behavior of materials across the weld interface, a scratch test was performed in this study. A diamond indenter was passed across the weld interface. A scratch test was conducted for each SOD in which the direction of the indenter was first moved from the Ti side to the SS side and from the SS side to the Ti side, respectively. The bidirectional scratch results are presented in Figs. 8 and 9, respectively. This approach enabled the investigation of the

material behavior during the transition from lower to higher hardness and vice versa. During the scratch test, when the indenter was moved from the Ti side to the SS side, the scratch width became shallower as a result of the higher resistance to plastic deformation shown by the harder SS compared to Ti. The average scratch widths obtained on the Ti side for different SODs of 5 mm, 10 mm, and 15 mm were 29.8 μm, 29.5 μm, and 29.0 μm, respectively, while on the SS side, they were 24.7 μm, 24.3 μm, and 23.2 μm, respectively. The decrease in scratch widths exhibited a correlation with the phenomenon of the work-hardening effect. Near the bonding interface on the Ti side, an oval shape was witnessed that exhibited divergent behavior followed by a convergent one. The scratch test results showed that an oval-shaped scratch morphology was observed at 10 μm from the weld interface in SOD-5 mm, while in the case of SOD-10 mm and 15 mm, it was observed at 15 μm and 24 μm, respectively. The formation of the oval shape near the weld interface is due to two main factors. Firstly, when the indenter moves from the Ti side to the SS side across the weld interface, a resistance force is developed at the interface due to differences in mechanical properties between

**Fig. 8** Scratch test from titanium to stainless steel side: **a** sample 1; **b** sample 2; **c** sample 3

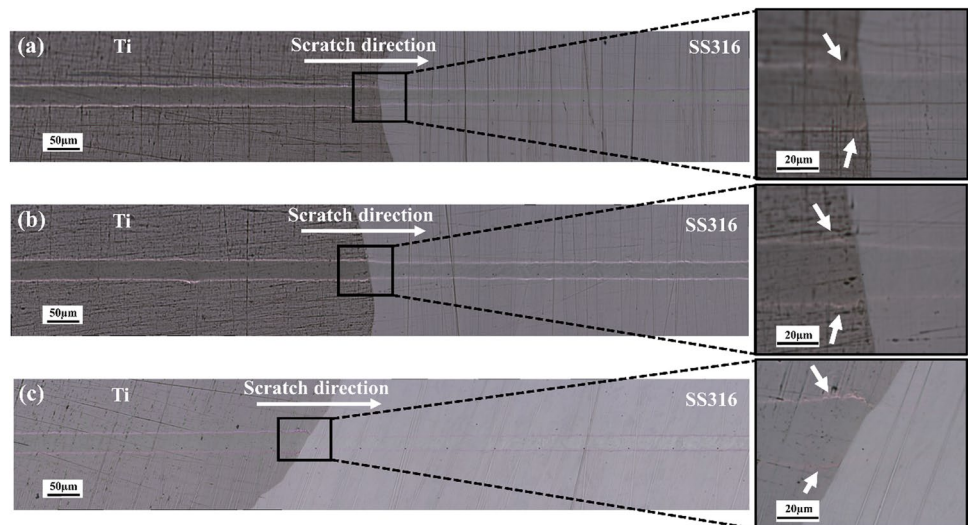
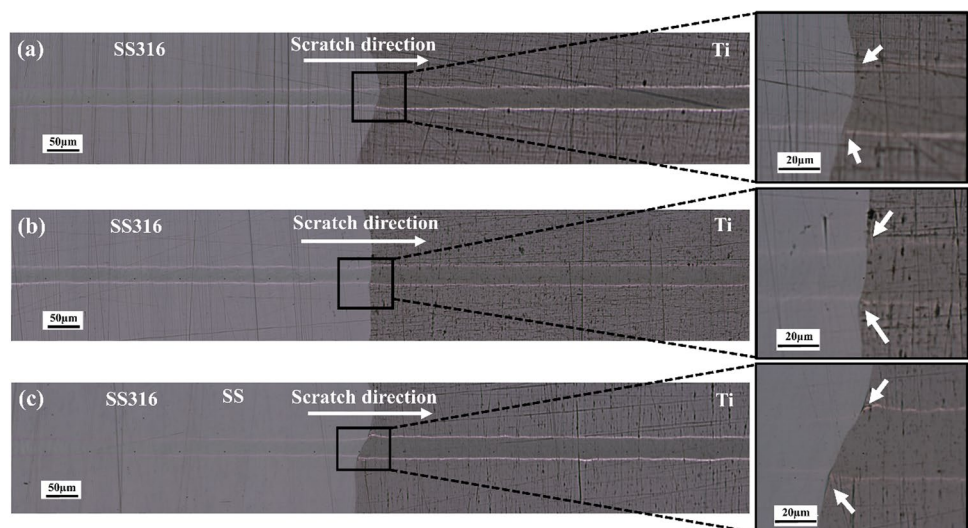


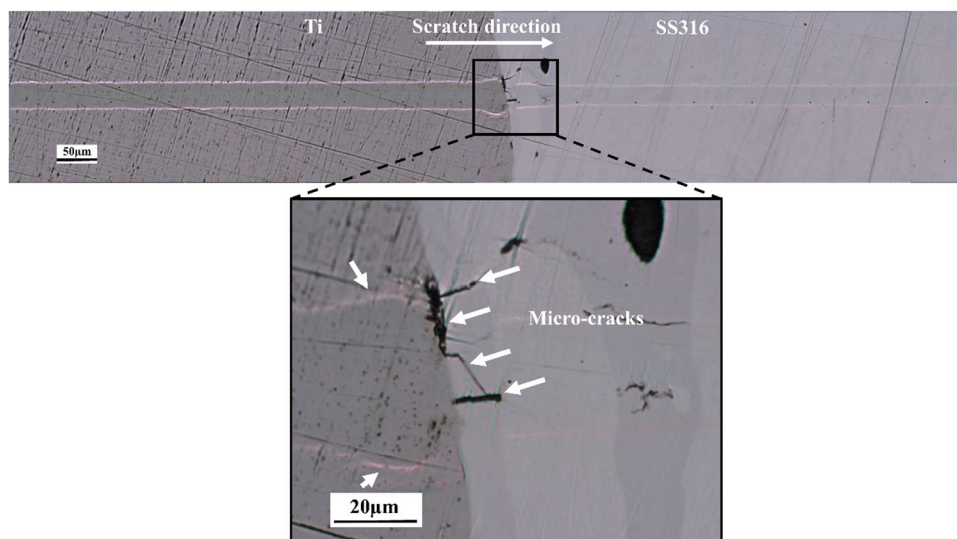
**Fig. 9** Scratch test from stainless steel to titanium side: **a** sample 1; **b** sample 2; **c** sample 3



the two materials. This resistance force increases due to the change in the strength of two materials, resulting in deformation. Secondly, the hardness value obtained near the weld interface can also contribute to this behavior. In the present study, both factors were observed. Similar interpretations were made when the indenter was moved from the SS to the Ti side, as there is an abrupt decrease in resistance due to the change in strength between the two materials. This decrease in resistance has caused the indenter to accelerate and potentially cause deformation on the Ti side near the interface. Moreover, the formation of an oval shape on the Ti side was less noticeable when the indenter was moved from the SS to the Ti side. The increase in scratch width just before the weld interface shows a decrease in the hardness value. This result is consistent with the hardness values obtained using the Vickers hardness test, which also showed a decrease in hardness value on the Ti side near the weld interface (Fig. 7).

During the scratch test in the vortex zone, the presence of microcracks was witnessed, as shown in Fig. 10. This was mainly due to the composition of the vortex zone, which consisted of a mixture of intermetallic compounds, oxides, and amorphous compounds. Manikandan et al. [36] have witnessed microcracks across the vortex. These microcracks were mainly due to residual stresses resulting from disparate heat transfer characteristics, intermetallic brittleness, shear stresses, and rapid cooling effects. Moreover, due to the presence of stronger and stiffer FeTi and Fe<sub>2</sub>Ti intermetallics, the microhardness test results of the vortices exhibited a significant difference in their hardness values. These components contributed to increased brittleness in the region, prominent to cracking [24]. Moreover, bidirectional scratch tests conducted on all clad materials showed no observable cracks at the bonding interface, demonstrating that clads welded at various SOD possessed robust mechanical properties and

**Fig. 10** Scratch test across the local melted zone in sample 3



could withstand various loading conditions. The bonding strength of the clad materials was subsequently evaluated and discussed in the following section.

### 3.2.3 Evaluation of the joint strength of Ti/SS316 clads

The evaluation of the bonding strength of welded plates is quite challenging. However, the use of focused ion beam (FIB) technology has facilitated the exploration of diverse ultra-small testing techniques for evaluating the mechanical properties of welded clads [44]. However, these techniques have some limitations, such as the high cost and significant expertise and skill required for sample preparation. In this study, a methodology for evaluating shear strength, similar to the one utilized by Xiang et al. [24], was employed to measure the bonding strength. Xiang et al. [24] have previously reported the shear strength of welded plates only in the longitudinal direction. However, in our study, we have thoroughly investigated the mechanical strength of the Ti/SS316 clads by implementing a tensile shear test in both longitudinal and transverse directions. The pre- and post-test tensile shear samples are shown in Fig. 11a, b, respectively. The results of the tensile shear test for both directions are shown in Fig. 11c, d, respectively. The results of the tensile shear test reveal that the explosively welded Ti/SS316 clads exhibit a shear load capacity that ranges from 352.7 to 404.6 MPa in the longitudinal direction and 295.7 to 359.3 MPa in the transverse direction (Table 2). The tensile shear strength of the composite was found to be greater than that of the base parent material, demonstrating that the explosively welded composite fulfils the requirements for a high-quality joint. Similar kinds of results were also documented by Acarer et al. [45] and Kaya and Kahraman [46] in their respective studies. In the longitudinal direction, the shear strength of the bonding interface increases from 393.0 MPa

for SOD-5 mm to 404.6 MPa for SOD-10 mm. A similar pattern is witnessed for the transverse direction, where the shear strength of the bonding interface increases from 347.5 MPa for SOD-5 mm to 359.3 MPa for SOD-10 mm. This enhancement in shear strength is due to the grain refinement, strain hardening, and strong interlocking that occur at the welding interface with an increase in SOD [47].

However, when the tensile shear strength was investigated at the higher SOD-15 mm, the results showed a decrease in the tensile shear strength of the welded clads in both longitudinal and transverse directions. The decrease in tensile shear strength was found to be 352.7 MPa and 295.7 MPa, respectively, for the longitudinal and transverse directions. The findings of the tensile shear strength investigation are in accordance with the findings of the microstructural study (Section 3.1), which showed the formation of various defects, including porosity, microcracks, and mixed zones, at the vortex of the weld interface. These defects act as stress concentration points, thereby degrading the mechanical properties of the composite material [48]. Moreover, the observed reduction in shear strength was found to be greater than the strength of the constituent materials of the composite. This is shown in Fig. 11e, where the fracture morphology of the tensile shear test is shown, indicating that fractures have occurred from the titanium side. These results suggest that the bonding strength of the Ti/SS316 clads was higher than the measured value. Similar kinds of results were also shown by Xiang et al. [24]. Additionally, the results of the tensile shear test show that both in the longitudinal and transverse directions, there is an increase in the shear strength with an increase in the SOD, as shown in Fig. 11f. It is noteworthy that the transformation in the tensile shear test values obtained for the longitudinal and transverse directions when shifting from SOD-5 mm to SOD-10 mm was nearly the same, with a difference of 11.6 MPa for

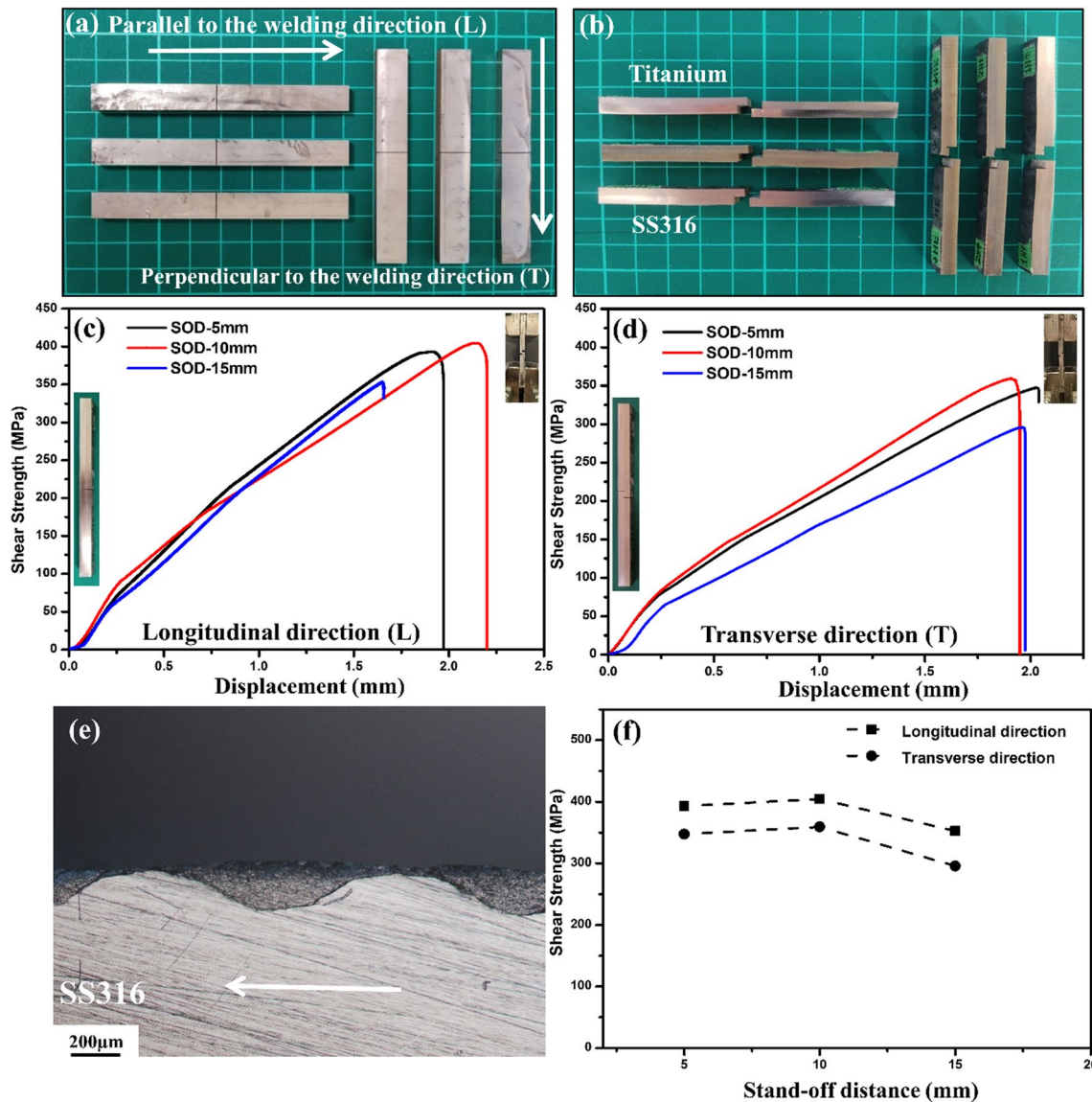


**Fig. 11** Tensile shear test results: **a** tensile shear samples before the test; **b** tensile shear samples after test; **c** shear strength value along the longitudinal direction; **d** shear strength value along the transverse

direction; **e** fracture morphology at SOD-15 in the longitudinal direction; **f** relationship between shear strength and SOD with the longitudinal and transverse direction

**Table 2** Tensile shear test results

Samples	Specimen along welding direction	Maximum shear strength /MPa
SOD-5 mm	Longitudinal	393.0
SOD-10 mm	Longitudinal	404.6
SOD-15 mm	Longitudinal	352.7
SOD-5 mm	Transverse	347.5
SOD-10 mm	Transverse	359.3
SOD-15 mm	Transverse	295.7

the longitudinal direction and 11.8 MPa for the transverse direction. However, the difference in the tensile shear test values when shifting from SOD-10 mm to SOD-15 mm was significant, with a difference of 51.9 MPa for the longitudinal direction and 63.6 MPa for the transverse direction. Additionally, at SOD-5 mm, the difference in the tensile shear test values obtained for the longitudinal and transverse directions was 45.5 MPa, while at SOD-10 mm, it was nearly the same at 45.3 MPa. However, at SOD-15 mm, the difference was 57 MPa. These findings specify that the shift from SOD-10 mm to SOD-15 mm has a significant impact on

the tensile shear strength of the composite material in both the longitudinal and transverse directions. A comparison of the tensile shear strength values for the longitudinal and transverse directions revealed that the shear strength value was higher in the longitudinal direction compared to the transverse direction. This finding aligns with previous results reported by Liangyu et al. [49] who conducted an explosive welding of TA1/304SS and witnessed a higher shear strength value in the longitudinal direction (350 MPa) compared to the transverse direction (309 MPa). These results highlight the influence of the directionality of the composite material on its tensile shear strength, emphasizing the need to consider the orientation of the composite material in applications where the mechanical properties are critical. The higher tensile shear strength in the longitudinal direction as compared to the transverse direction can be attributed to the formation of front vortices in the longitudinal direction, which results in improved mechanical bonding between the flyer and base material [34].

### 3.2.4 Fracture analysis

The results of the tensile shear tests have confirmed that the explosively welded Ti/SS316 clads had good shear strength. To further understand the failure mechanism of the welded specimen, SEM fractography of the fractured samples was done. Tian et al. [50] have shown that the microstructure of the weld interface shows a well-defined wave bonding

structure when observed along the longitudinal direction. Furthermore, an irregular, undulating weld interface was witnessed in the transverse direction. SEM fractography, as represented in Fig. 12, demonstrated that the mode of fracture in the longitudinal direction is a combination of ductile and brittle fracture. Figure 12a shows the fractography behavior of the sample subjected to a tensile shear test at SOD-5 mm, where the presence of numerous shear-elongated dimples can be observed. Furthermore, when the SOD was increased to 10 mm, more intense shear-elongated dimples were observed, as shown in Fig. 12b, indicating significant plastic deformation before fracture. This is consistent with the fact that at this SOD, the highest tensile shear test value was obtained (Table 2). Venkateswara Rao et al. [51] stated in their study that good shear strength was accomplished when the fracture mode was dimpled rupture. At SOD-15 mm (Fig. 12c), the presence of tear ridges, voids, dimples, and cleavage planes on the fracture surface was observed. This can be correlated with the fact that the tensile shear test value obtained at this point was lower than the value obtained at SOD-10 mm. The cleavage plane also indicates that the material has undergone a brittle fracture. This brittle fracture is the result of a high degree of shock hardening which has occurred during explosive welding at the weld interface [48]. Similarly, SEM fractography for the tensile shear test in the transverse direction is presented in Fig. 13, which also reveals the mode of failure in the material was the combination of both ductile and brittle fractures. At an

**Fig. 12** Fractography of tensile shear test samples along the longitudinal direction: **a** sample 1; **b** sample 2; **c** sample 3

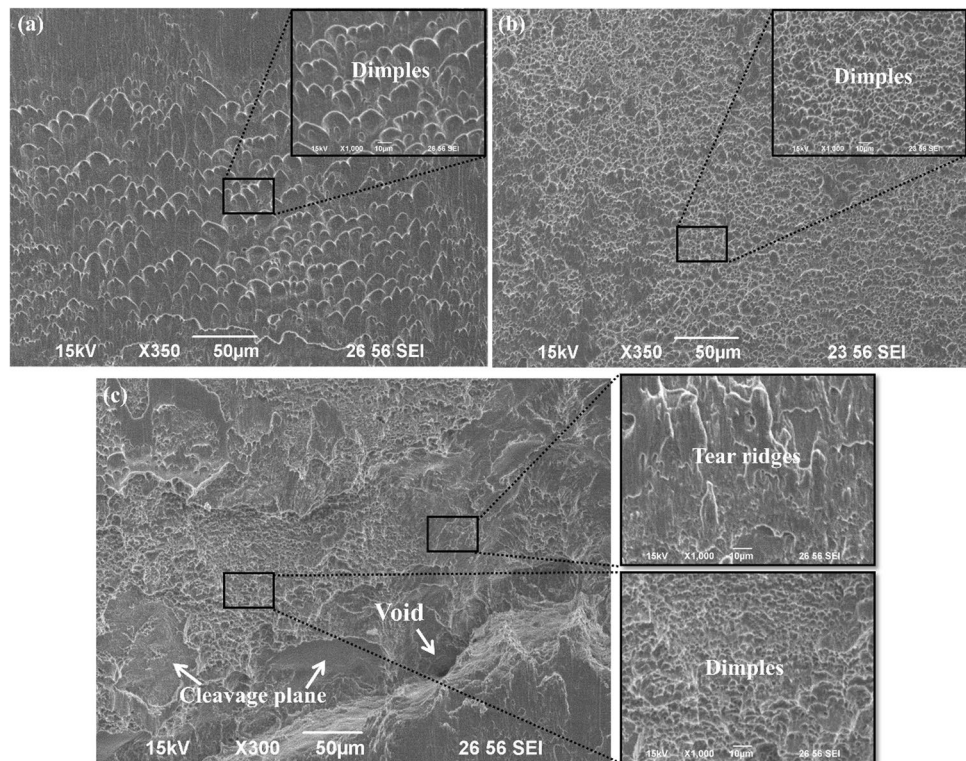
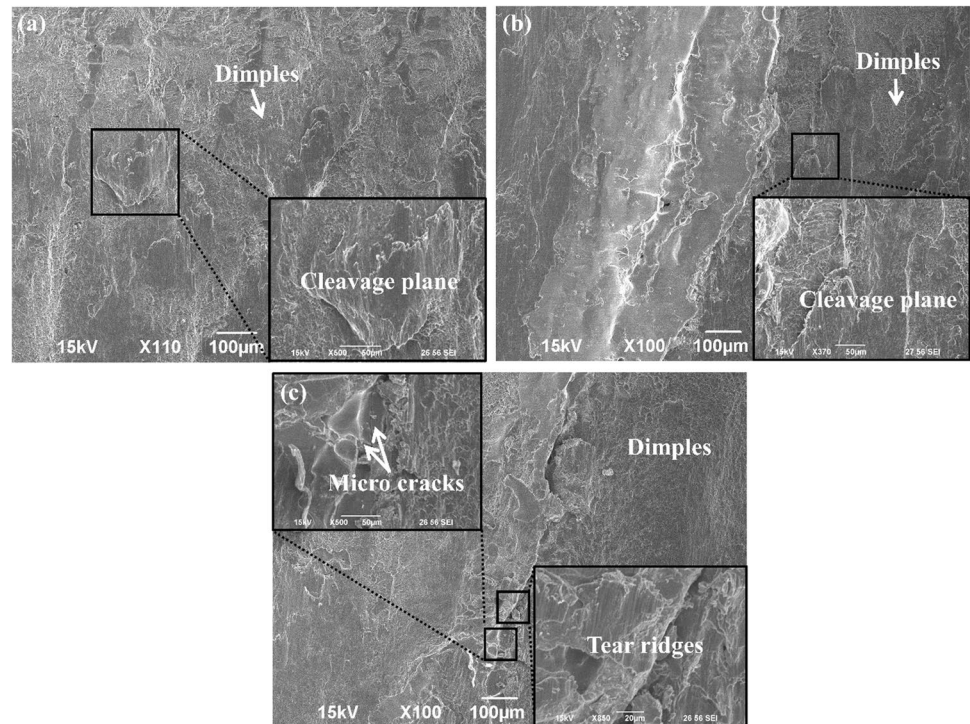


**Fig. 13** Fractography of tensile shear test samples along the transverse direction: **a** sample 1; **b** sample 2; **c** sample 3



SOD-5 mm, the formation of dimples and a cleavage plane can be observed, as shown in Fig. 13a. At SOD-10 mm, it resulted in a higher density of dimples and cleavage planes, as presented in Fig. 13b, signifying the occurrence of both ductile and brittle failure at the surface. Figure 13c demonstrated the formation of microcracks, dimples, and tear ridges, largely due to the poor toughness and high impact developed during the explosive welding process [52].

## 4 Conclusions

In this research work, clads comprising pure commercial titanium (TP 270C) and stainless steel (SS316) were successfully fabricated using an explosive welding process. Subsequently, an extensive investigation was conducted to thoroughly explore and characterize the microstructural and mechanical properties of these weld clads. The acquired data and analysis from this study led to the following noteworthy conclusions:

1. The microstructure of the welding interface changes with increasing SOD. At low SOD-5 mm, a clear, wavy interface with negligible defects was witnessed. At SOD-10 mm, a non-uniform local melted zone at the weld interface was observed. At SOD-15mm, a wavy morphology with vortices, melted zones, and porosity was witnessed in the welding region. As SOD increases, dynamic impact and kinetic energy also increase, resulting in microcracks perpendicular to the welding interface.
2. Higher SOD leads to an increase in wavelength and amplitude, but the wavelength shows greater variation compared to the amplitude. EPMA shows that the porosity was likely to act in the peninsula and island morphologies near the welding zone.
3. The scratch results showed that an oval-shaped scratch morphology was observed near the weld interface, which increased with an increase in SOD. This suggests that the recrystallization distance near the weld interface increases with an increase in SOD. The formation of the oval shape can be attributed to differences in mechanical properties between the two materials and a decrease in the hardness value near the weld interface.
4. The tensile shear test was measured in two different directions at three different levels of deformation (SOD-5 mm, SOD-10 mm, and SOD-15 mm). Higher tensile shear strength was witnessed in the longitudinal direction as compared to the transverse direction. The results showed that the difference in strength between the two directions was small when the level of deformation changed from SOD-5 mm to SOD-10 mm but decreased significantly when it changed from SOD-10 mm to SOD-15 mm. These results provide important insights into the microstructural characteristics of the explosively welded Ti/SS316 clads and suggest that the longitudinal direction is more favorable for achieving good mechanical bonding than the transverse direction.
5. SEM fractography showed that the fracture mode in the longitudinal direction of a material subjected to tensile

shear tests is a combination of ductile and brittle fracture. An increase in SOD leads to an increase in the intensity of plastic deformation. The transverse direction also showed evidence of both ductile and brittle failures, as well as microcracks and tear ridges due to poor toughness and high impact from explosive welding.

The study established a noteworthy correlation between the stand-off distance (SOD) and the resultant weld characteristics in Ti/SS316 clads, indicating the critical influence of this parameter. By extensively scrutinizing the microstructural and mechanical properties, an SOD of 10 mm was identified as the optimal welding parameter, leading to superior weld quality in the fabricated weld clads.

**Acknowledgements** We would like to sincerely thank Mr. Minghong Yu and Mr. Atsushi Onohara, master's degree students at the Graduate School of Science and Technology at Kumamoto University, for their help and generous assistance during the experimental process. We would also like to thank Mr. Zhihong Dai and Mr. Kang Jiang, master's degree students at the Graduate School of Science and Technology at Kumamoto University, for their generous support in the scratch test.

**Author contribution** Bir Bahadur Sherpa: investigation, methodology, validation, writing-original draft preparation, and writing-review and editing. Masatoshi Kuroda: conceptualization. Tomohiro Ikeda: resources. Koji Kawamura: resources. Daisuke Inao: investigation and resources. Shigeru Tanaka: supervision and resources. Kazuyuki Hokamoto: conceptualization, resources, supervision, and writing-review and editing. All authors read and approved the final manuscript.

**Funding** This study was funded by the Institute of Industrial Nanomaterials, Kumamoto University (no grant numbers).

**Data availability** The authors confirm that the data and material supporting the findings of this work are available within the article.

## Declarations

**Ethical approval** The article follows the guidelines of the Committee on Publication Ethics (COPE) and involves no studies on human or animal subjects.

**Consent to participate** Not applicable. The article involves no studies on humans.

**Consent for publication** Not applicable. The article involves no studies on humans.

**Competing interests** The authors declare no competing.

## References

- Nieslony P, Cichosz P, Krolczyk G, Legutko S, Smyczek D, Kolodziej M (2016) Experimental studies of the cutting force and surface morphology of explosively clad Ti–steel plates. *Measurement* 78:129–1371. <https://doi.org/10.1016/j.measurement.2015.10.005>
- Song X, Wang L, Wang R, Liu Y (2022) Effects of annealing on microstructure evolution and mechanical properties of constrained groove pressed pure titanium. *Mater Sci Eng A* 831:142245. <https://doi.org/10.1016/j.msea.2021.142245>
- Gupta R, Birbilis N (2015) The influence of nanocrystalline structure and processing route on corrosion of stainless steel: a review. *Corros Sci* 92:1–15. <https://doi.org/10.1016/j.corsci.2014.11.041>
- Mousavi SA, Sartangi PF (2008) Effect of post-weld heat treatment on the interface microstructure of explosively welded titanium–stainless steel composite. *Mater Sci Eng A* 494(1–2):329–336. <https://doi.org/10.1016/j.msea.2008.04.032>
- Song J, Kostka A, Veehmayer M, Raabe D (2011) Hierarchical microstructure of explosive joints: Example of titanium to steel cladding. *Mater Sci Eng A* 528(6):2641–2647. <https://doi.org/10.1016/j.msea.2010.11.092>
- Xia Y, Dong H, Hao X, Li P, Li S (2019) Vacuum brazing of Ti6Al4V alloy to 316L stainless steel using a Ti–Cu–based amorphous filler metal. *J Mater Process Technol* 269:35–44. <https://doi.org/10.1016/j.jmatprotec.2019.01.020>
- Chen H-C, Bi G, Lee BY, Cheng CK (2016) Laser welding of CP Ti to stainless steel with different temporal pulse shapes. *J Mater Process Technol* 231:58–65. <https://doi.org/10.1016/j.jmatprotec.2015.12.016>
- Cheepu M, Ashfaq M, Muthupandi V (2017) A new approach for using interlayer and analysis of the friction welding of titanium to stainless steel. *Trans Indian Inst Met* 70(10):2591–2600. <https://doi.org/10.1007/s12666-017-1114-x>
- Li Y-I, Di H-s, Li T-x, Chen L-q, Wang X-n, Misra R (2022) Effect of thickness of transition layer on the microstructure and properties of the titanium/stainless steel welds with oscillating laser. *J Mater Res Technol* 18:210–222. <https://doi.org/10.1016/j.jmrt.2022.02.064>
- Zhang Y, Sun D, Gu X, Li H (2018) Nd: YAG pulsed laser welding of dissimilar metals of titanium alloy to stainless steel. *Int J Adv Manuf Technol* 94(1):1073–1085. <https://doi.org/10.1007/s00170-017-0997-3>
- Hokamoto K, Chiba A, Fujita M, Izuma T (1995) Single-shot explosive welding technique for the fabrication of multilayered metal base composites: effect of welding parameters leading to optimum bonding condition. *Compos Eng* 5(8):1069–1079. [https://doi.org/10.1016/0961-9526\(95\)00059-V](https://doi.org/10.1016/0961-9526(95)00059-V)
- Sherpa BB, Kumar PD, Upadhyay A, Kumar S, Agarwal A, Tyagi S (2020) Low velocity of detonation explosive welding (LVEW) process for metal joining. *Propellants Explos Pyrotech* 45(10):1554–1565. <https://doi.org/10.1002/prep.202000019>
- Findik F (2011) Recent developments in explosive welding. *Mater Des* 32(3):1081–1093. <https://doi.org/10.1016/j.matdes.2010.10.017>
- Sherpa BB, Kumar PD, Upadhyay A, Kumar S, Agarwal A, Tyagi S (2021) Experimental and theoretical study of dynamic bend angle in the explosive welding process. *Trans Indian Inst Met* 74:511–519. <https://doi.org/10.1007/s12666-021-02189-7>
- Hokamoto K, Izuma T, Fujita M (1993) New explosive welding technique to weld aluminum alloy and stainless steel plates using a stainless steel intermediate plate. *Metall Trans A* 24(10):2289–2297. <https://doi.org/10.1007/BF02648602>
- Mousavi SA, Sartangi PF (2009) Experimental investigation of explosive welding of cp-titanium/AISI 304 stainless steel. *Mater Des* 30(3):459–468. <https://doi.org/10.1016/j.matdes.2008.06.016>
- Prasanthi TN, C Sudha R, Saroja S (2016) Explosive cladding and post-weld heat treatment of mild steel and titanium. *Mater Des* 93:180–193. <https://doi.org/10.1016/j.matdes.2015.12.120>
- Chu Q, Zhang M, Li J, Yan C (2017) Experimental and numerical investigation of microstructure and mechanical behavior of titanium/steel interfaces prepared by explosive welding. *Mater Sci Eng A* 689:323–331. <https://doi.org/10.1016/j.msea.2017.02.075>
- Zhou Q, Liu R, Ran C, Fan K, Xie J, Chen P (2022) Effect of microstructure on mechanical properties of titanium–steel

- explosive welding interface. *Mater Sci Eng A* 830:142260. <https://doi.org/10.1016/j.msea.2021.142260>
20. Soltani HM, Tayebi M (2018) Comparative study of AISI 304L to AISI 316L stainless steels joints by TIG and Nd: YAG laser welding. *J Alloys Compd* 767:112–121. <https://doi.org/10.1016/j.jallcom.2018.06.302>
  21. Beake B, Vishnyakov V, Harris A (2017) Nano-scratch testing of (Ti, Fe) Nx thin films on silicon. *Surf Coat Technol* 309:671–679. <https://doi.org/10.1016/j.surfcoat.2016.11.024>
  22. Küster RL, Schiffmann KI (2022) Nano-scratch testing on thin diamond-like carbon coatings for microactuators: friction, wear and elastic-plastic deformation. *Int J Mater Res* 95(5):306–310. <https://doi.org/10.3139/ijmr-2004-0066>
  23. Marian M, Berman D, Nečas D, Emani N, Ruggiero A, Rosenkranz A (2022) Roadmap for 2D materials in biotribological/ biomedical applications—a review. *Adv Colloid Interface Sci* 307:102747. <https://doi.org/10.1016/j.cis.2022.102747>
  24. Xiang C, Daisuke I, Tanaka S, Li X-j, Bataev I, Hokamoto K (2021) Comparison of explosive welding of pure titanium/SUS 304 austenitic stainless steel and pure titanium/SUS 821L1 duplex stainless steel. *T Nonferr Metal Soc* 31(9):2687–2702. [https://doi.org/10.1016/S1003-6326\(21\)65685-6](https://doi.org/10.1016/S1003-6326(21)65685-6)
  25. Chu Q, Tong X, Xu S, Zhang M, Li J, Yan F, Yan C (2020) Interfacial investigation of explosion-welded titanium/steel bimetallic plates. *J of Materi Eng and Perform* 29(1):78–86. <https://doi.org/10.1007/s11665-019-04535-9>
  26. Deo M, Tewari S, Mahobia G (2020) Behaviour of haz and weld bead under different welding condition for A572 Gr 50 steel. *Int J Adv Res. Eng Technol* 11(6). <https://doi.org/10.34218/IJARET.11.6.2020.059>
  27. Tian Q, Yang M, Xu J, Ma H, Zhao Y, Shen Z, Ren Z, Zhou H, Tian J (2022) Microstructure evolution and mechanical property of W/Ta bimetal foil produced by a high wave impedance explosive welding technology. *Int J Adv Manuf Technol* 120(1-2):1023–1040. <https://doi.org/10.1007/s00170-021-08502-4>
  28. Athar MH, Tolaminejad B (2015) Weldability window and the effect of interface morphology on the properties of Al/Cu/Al laminated composites fabricated by explosive welding. *Mater Des* 86:516–525. <https://doi.org/10.1016/j.matdes.2015.07.114>
  29. Bahrani A, Black T, Crossland B (1967) The mechanics of wave formation in explosive welding. *Proc R Soc Lond* 296(1445):123–136. <https://doi.org/10.1098/rspa.1967.0010>
  30. Zhang L-J, Pei Q, Zhang J-X, Bi Z-Y, Li P-C (2014) Study on the microstructure and mechanical properties of explosive welded 2205/X65 bimetallic sheet. *Mater Des* 64:462–476. <https://doi.org/10.1016/j.matdes.2014.08.013>
  31. Gloc M, Wachowski M, Plocinski T, Kurzydowski KJ (2016) Microstructural and microanalysis investigations of bond titanium grade1/low alloy steel st52-3N obtained by explosive welding. *J Alloys Compd* 671:446–451. <https://doi.org/10.1016/j.jallcom.2016.02.120>
  32. Yang M, Xu J, Ma H, Lei M, Ni X, Shen Z, Zhang B, Tian J (2021) Microstructure development during explosive welding of metal foil: morphologies, mechanical behaviors and mechanisms. *Compos B Eng* 212:108685. <https://doi.org/10.1016/j.compositesb.2021.108685>
  33. Pei Y, Huang T, Chen F, Pang B, Guo J, Xiang N, Song Z, Zhang Y (2020) Microstructure and fracture mechanism of Ti/Al layered composite fabricated by explosive welding. *Vacuum* 181:109596. <https://doi.org/10.1016/j.vacuum.2020.109596>
  34. Durgutlu A, Okuyucu H, Gulenc B (2008) Investigation of effect of the stand-off distance on interface characteristics of explosively welded copper and stainless steel. *Mater Des* 29(7):1480–1484. <https://doi.org/10.1016/j.matdes.2007.07.012>
  35. Wang J, Li X-j, Yan H-h, Wang X-h, Wang Y-x (2022) Research on titanium-copper explosive welding interface with different welding parameters. *Int J Adv Manuf Technol* 122(9):3595–3606. <https://doi.org/10.1007/s00170-022-10102-9>
  36. Manikandan P, Hokamoto K, Deribas AA, Raghukandan K, Tomoshige R (2006) Explosive welding of titanium/stainless steel by controlling energetic conditions. *Mater Trans* 47(8):2049–2055. <https://doi.org/10.2320/matertrans.47.2049>
  37. Pouraliakbar H, Khalaj G, Jandaghi MR, Fadaei A, Ghareh-Shiran MK, Shim SH, Hong SI (2020) Three-layered SS321/AA1050/AA5083 explosive welds: effect of PWHT on the interface evolution and its mechanical strength. *Int J Press Vessel Pip* 188:104216. <https://doi.org/10.1016/j.ijpvp.2020.104216>
  38. Bataev I, Lazurenko D, Tanaka S, Hokamoto K, Bataev A, Guo Y, Jorge A Jr (2017) High cooling rates and metastable phases at the interfaces of explosively welded materials. *Acta Mater* 135:277–289. <https://doi.org/10.1016/j.actamat.2017.06.038>
  39. Chen X, Inao D, Li X, Tanaka S, Li K, Hokamoto K (2022) Optimal parameters for the explosive welding of TP 270C pure titanium and SUS 821L1 duplex stainless steel. *J Mater Res Technol* 19:4771–4786. <https://doi.org/10.1016/j.jmrt.2022.07.031>
  40. Paul H, Skuza W, Chulist R, Miszczyk M, Gałka A, Prazmowski M, Pstruś J (2020) The effect of interface morphology on the electro-mechanical properties of Ti/Cu clad composites produced by explosive welding. *Metall Mater Trans A* 51:750–766. <https://doi.org/10.1007/s11661-019-05537-x>
  41. Saravanan S, Inokawa H, Tomoshige R, Raghukandan K (2020) Microstructural characterization of silicon carbide reinforced dissimilar grade aluminium explosive clads. *Def Technol* 16(3):689–694. <https://doi.org/10.1016/j.dt.2019.10.008>
  42. Sherpa BB, Kumar PD, Upadhyay A, Kumar S, Agarwal A, Tyagi S (2021) Effect of explosive welding parameters on Al/LCS interface clad by low velocity of detonation explosive welding (LVEW) process. *Int J Adv Manuf Technol* 113(11):3303–3317. <https://doi.org/10.1007/s00170-021-06800-5>
  43. Zhao H, Sheng L (2021) Microstructure and mechanical properties of the Ag/316L composite plate fabricated by explosive welding. *J Manuf Process* 64:265–275. <https://doi.org/10.1016/j.jmapro.2021.01.026>
  44. Wu X, Kondo S, Yu H, Okuno Y, Ando M, Kurotaki H, Tanaka S, Hokamoto K, Ochiai R, Konishi S (2021) Bonding strength evaluation of explosive welding joint of tungsten to ferritic steel using ultra-small testing technologies. *Mater Sci Eng A* 826:141995. <https://doi.org/10.1016/j.msea.2021.141995>
  45. Acarer M, Gülenç B, Findik F (2003) Investigation of explosive welding parameters and their effects on microhardness and shear strength. *Mater Des* 24(8):659–664. [https://doi.org/10.1016/S0261-3069\(03\)00066-9](https://doi.org/10.1016/S0261-3069(03)00066-9)
  46. Kaya Y, Kahraman N (2013) An investigation into the explosive welding/cladding of grade A ship steel/AISI 316L austenitic stainless steel. *Mater Des* 1980-2015(52):367–372. <https://doi.org/10.1016/j.matdes.2013.05.033>
  47. Mastanaiah P, Reddy GM, Prasad KS, Murthy C (2014) An investigation on microstructures and mechanical properties of explosive clad C103 niobium alloy over C263 nimonic alloy. *J Mater Process Technol* 214(11):2316–2324. <https://doi.org/10.1016/j.jmatprotec.2014.04.025>
  48. Zhou Q, Liu R, Fan K, Xie J, Chen P, Rittel D (2022) Tensile behavior of the titanium-steel explosive welded interface under quasi-static and high-strain rate loading. *Int J Solids Struct* 254:111870. <https://doi.org/10.1016/j.ijso.2022.111870>
  49. Liangyu L, Yong S, Jian C, Yu F, Xiaoyuan X, Jin Y (2020) Study on microstructure and properties of TA1-304 stainless steel explosive welding cladding plate. *Mater Res Express* 7(2):026557. <https://doi.org/10.1088/2053-1591/ab7357>

50. Tian Q, Sun Y, Ma H, Zhao Y, Shen Z, Ren Z, Zhou H, Tian J, Fu S (2021) Performance of fine-grained W/Cu plate prepared by explosive welding with high wave impedance confinement at room temperature. *Fusion Eng Des* 172:112855. <https://doi.org/10.1016/j.fusengdes.2021.112855>
51. Venkateswara Rao N, Madhusudhan Reddy G, Nagarjuna S (2014) Structure and properties of explosive clad HSLA steel with titanium. *Trans Indian Inst Met* 67:67–77. <https://doi.org/10.1007/s12666-013-0313-3>
52. Zhou Q, Liu R, Chen P, Zhu L (2021) Microstructure characterization and tensile shear failure mechanism of the bonding interface of explosively welded titanium-steel composite. *Mater Sci Eng A* 820:141559. <https://doi.org/10.1016/j.msea.2021.141559>

**Publisher's note** Springer Nature remains neutral with regard to jurisdictional claims in published maps and institutional affiliations.

Springer Nature or its licensor (e.g. a society or other partner) holds exclusive rights to this article under a publishing agreement with the author(s) or other rightsholder(s); author self-archiving of the accepted manuscript version of this article is solely governed by the terms of such publishing agreement and applicable law.